



Simulating non-completely positive actions via exponentiation of Hermitian-preserving maps



Fuchuan Wei ^{1,6}, Zhenhuan Liu ^{2,6}, Guoding Liu ², Zizhao Han², Dong-Ling Deng ^{2,3,4} ✉ & Zhengwei Liu ^{1,5} ✉

Legitimate quantum operations must adhere to principles of quantum mechanics, particularly the requirements of complete positivity and trace preservation. Yet, non-completely positive maps, especially Hermitian-preserving maps, play a crucial role in quantum information science. Here, we introduce the Hermitian-preserving map exponentiation algorithm, which can effectively simulate the action of an arbitrary Hermitian-preserving map by exponentiating its output, $\mathcal{N}(\rho)$, into a quantum process, $e^{-i\mathcal{N}(\rho)t}$. We analyze the sample complexity of this algorithm and prove its optimality in certain cases. Utilizing positive but not completely positive maps, this algorithm provides exponential speedups in entanglement detection and quantification compared to protocols based on single-copy operations. In addition, it facilitates the encoding-free recovery of noiseless quantum states from multiple noisy ones by simulating the inverse map of the corresponding noise channel, providing a new approach to handling quantum noises. This algorithm acts as a building block of large-scale quantum algorithms and presents a pathway for exploring potential quantum speedups across a wide range of information-processing tasks.

Principles of quantum mechanics dictate that quantum operations must act on and output density matrices, which are positive matrices with a unit trace¹. Thus, a valid quantum operation, known as a quantum channel, must be completely positive and trace-preserving (CPTP). As depicted in Fig. 1a, the set of CPTP maps represents only a small subset of all linear maps². In practice, many quantum tasks require non-completely positive (non-CP) maps beyond the scope of CPTP requirements, including entanglement detection³ and quantum error mitigation^{4,5}.

In entanglement detection and quantification, positive but not completely positive maps³ serve as crucial tools. For instance, the positive partial transposition criterion⁶, based on the transposition map, is widely employed for entanglement detection^{7,8} and distillation⁹. Moreover, the entanglement negativity, which quantifies the violation of the positive partial transposition criterion, represents an easily computable and operationally meaningful entanglement measure³. However, due to their lack of complete positivity, verifying the positive map criterion often requires highly joint operations or exponential repetition times^{7,10,11}. In quantum error mitigation^{4,5}, inverse maps of noise channels are generally non-CP, techniques such as probabilistic error cancellation^{12–14} are adopted to statistically realize these

inverse maps. These approaches only recover noiseless expectation values rather than noiseless states, limiting the range of applications.

Given the importance of non-CP maps, especially Hermitian-preserving (HP)¹⁵ ones as exemplified above, researchers have devoted substantial efforts to find their implementations^{16–20}. For example, methods based on structural approximation^{21,22} and Petz recovery map^{23,24} employ quantum channels to approximate non-CP maps. However, many non-CP maps are far from the set of CPTP maps and cannot be implemented effectively with these methods. The multi-copy extension method²⁵ utilizes a joint quantum channel acting on multiple copies of input states to produce a single output of the non-CP map, which is feasible only when the output remains a density matrix. As shown, existing approaches are restricted in the level of quantum states and aim to prepare outputs of non-CP maps in some indirect ways. Since the output of a non-CP map is not always a density matrix, these approaches face fundamental limitations in efficiency and feasibility.

In this paper, we go beyond the level of quantum states and propose a novel approach to effectively simulate the actions of all HP maps. To circumvent the restriction posed on quantum operations, our core idea is to

¹Yau Mathematical Sciences Center and Department of Mathematics, Tsinghua University, 100084 Beijing, PR China. ²Center for Quantum Information, Institute for Interdisciplinary Information Sciences, Tsinghua University, 100084 Beijing, PR China. ³Shanghai Qi Zhi Institute, 41th Floor, AI Tower, No. 701 Yunjin Road, Xuhui District, Shanghai, 200232, PR China. ⁴Hefei National Laboratory, Hefei, 230088, PR China. ⁵Yanqi Lake Beijing Institute of Mathematical Sciences and Applications, 100407 Beijing, PR China. ⁶These authors contributed equally: Fuchuan Wei, Zhenhuan Liu. ✉ e-mail: dldeng@tsinghua.edu.cn; liuzhengwei@mail.tsinghua.edu.cn

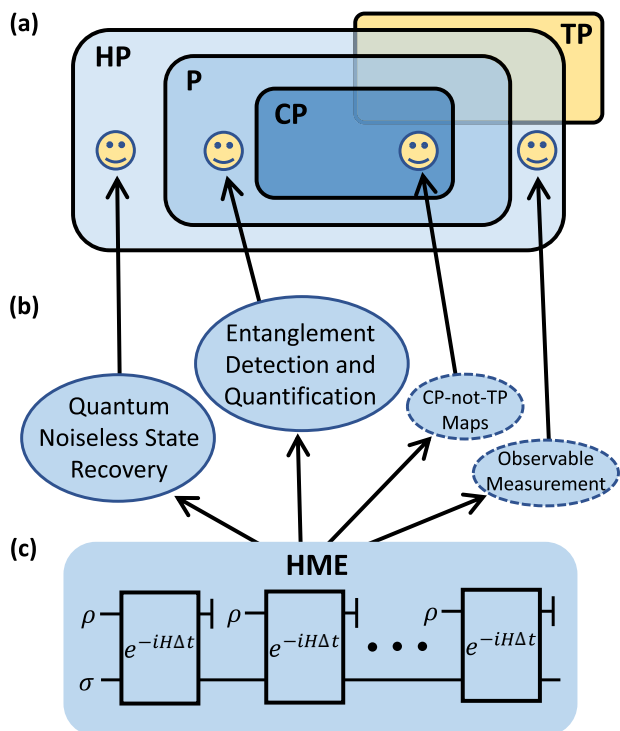


Fig. 1 | Overview of Hermitian-preserving map exponentiation algorithm. a Diagrammatic representation of different types of maps, including CP (completely positive), P (positive), HP (Hermitian-preserving), and TP (trace-preserving) maps. Physical maps lie in the intersection of CP and TP. The smiling faces represent the maps used in the four applications listed in b. These applications are all situated within the HP maps region, among which we extensively explore entanglement detection and quantification, as well as quantum noiseless state recovery. c Circuit diagram for Hermitian-preserving map exponentiation, comprising three components: sequential input of identical states ρ , the evolved state σ preserved using quantum memory, and joint Hamiltonian evolution.

change the carrier of the output of non-CP maps. More concretely, as the output of a HP map, $\mathcal{N}(\rho)$, is a Hermitian matrix, we can transform it into the Hamiltonian that determines the evolution of a physical system. Therefore, by “exponentiating” a HP map, we define a new map $e^{-i\mathcal{N}(\cdot)t}$. This new map maps an arbitrary input state ρ to a unitary evolution $e^{-i\mathcal{N}(\rho)t}$, which contains all information of $\mathcal{N}(\rho)$. With techniques including Hadamard test and quantum phase estimation, the information of $\mathcal{N}(\rho)$ can be extracted from $e^{-i\mathcal{N}(\rho)t}$. With this approach, we transform a HP map from a purely mathematical object into a physical process that can be implemented in the laboratory.

To realize the map $e^{-i\mathcal{N}(\cdot)t}$, we design a quantum algorithm, *Hermitian-preserving map exponentiation* (HME), as depicted in Fig. 1c. The density matrix exponentiation algorithm^{26,27}, which has been proved to exhibit exponential speedup compared to single-copy strategies in certain tasks²⁸, is a special case of HME when \mathcal{N} is the identity map. We analyze the performances of HME and prove its optimality in sample complexity for simulating certain non-CP maps. Given that HP maps are significantly more general than CPTP maps and encompass a wide range of crucial non-CP maps, HME has the potential to be a key tool in various quantum information processing tasks. One direct application of HME lies in entanglement detection and quantification, as positive maps are HP. In entanglement detection, we incorporate HME into the quantum phase estimation algorithm^{1,29} to propose a new entanglement detection protocol. We demonstrate through an example that the HME-based protocol can offer exponential speedups compared to all single-copy approaches. Moreover, by combining the HME and Hadamard test algorithm³⁰, we develop a protocol to estimate entanglement negativity and compare it to conventional means, showcasing advantages in resource consumption.

Another significant application is quantum noiseless state recovery, which relies on the ability of HME to simulate the inverse map of a noise channel. We integrate HME into a simple quantum circuit to recover the noiseless state with arbitrary precision and analyze its performance. This protocol can handle any invertible noise when the description of the noise channel is known. In contrast to existing methods such as quantum error mitigation and quantum error correction, our protocol can recover the desired noiseless state from multiple noisy states, establishing a new approach for combating quantum noises.

Results

Hermitian-preserving map exponentiation

The circuit of HME is sketched in Fig. 1c. To implement the evolution of $e^{-i\mathcal{N}(\rho)t}$ on the state σ , the HME algorithm begins with preparing two quantum systems. The target state ρ will be prepared on the first system, while the second system serves as a quantum memory to keep the state on which the evolution of $e^{-i\mathcal{N}(\rho)t}$ is applied. In the beginning, the quantum memory is prepared in the initial state σ . Based on the desired accuracy, the HP map \mathcal{N} , and the total evolution time t , one determines an appropriate Hamiltonian H and a short time period Δt according to Theorem 1 and Theorem 2, respectively. Subsequently, one repeats the following steps for a total of $K = t/\Delta t$ times and realizes $e^{-i\mathcal{N}(\rho)t}$ on the second system in the end:

1. Prepare the target state ρ on the first system.
2. Evolve the two systems jointly using $e^{-iH\Delta t}$ and discard the state on the first system.

Below, we introduce Theorem 1 to show how to choose Hamiltonian H to realize HP map \mathcal{N} .

Theorem 1. (Validation of HME). For a short time period Δt , we have

$$\text{Tr}_1(e^{-iH\Delta t}(\rho \otimes \sigma)e^{iH\Delta t}) = e^{-i\mathcal{N}(\rho)\Delta t}\sigma e^{i\mathcal{N}(\rho)\Delta t} + \mathcal{O}(\Delta t^2). \quad (1)$$

Here, Tr_1 denotes the partial trace over the first system, \mathcal{N} represents the target HP map, $H = \Lambda_{\mathcal{N}}^{\text{T}_1}$ with $\Lambda_{\mathcal{N}} = (\mathcal{I} \otimes \mathcal{N})|\Phi^+\rangle\langle\Phi^+|$ being the Choi matrix for \mathcal{N} , $|\Phi^+\rangle = \sum_i |ii\rangle$ denotes the unnormalized maximally entangled state, and T_1 represents the partial transposition operation on the first system.

This theorem can be proved using Taylor expansion and tensor network representation in Fig. 2a, b. In general, the calculation of H using \mathcal{N} is complicated. However, in many practical applications, \mathcal{N} has certain structures that benefit the calculation of H . An illustrative example is the partial transposition map $e^{-i\rho^{\text{T}_A}t}$, where ρ is a bipartite state with two subsystems A and B . According to Theorem 1, the corresponding Hamiltonian for HME is given by $H_p = \Phi_A^+ \otimes S_B$, which has a qubit-wise tensor product form and is depicted within the red dashed box in Fig. 2c. The two blue half circles within the box represent the unnormalized maximally entangled state Φ_A^+ , while the cross of purple lines represents the SWAP operator S_B . We can deduce the validity of $\text{Tr}_1([H_p, \rho \otimes \sigma]) = [\rho^{\text{T}_A}, \sigma]$ based on the connection rule of the legs.

According to Theorem 1, the difference between the ideal and real channels for a single step of the experiment is a second-order term. Thus the error of the whole process could be suppressed by choosing a smaller time slice Δt , or equivalently, by using more copies of ρ .

Sample complexity analysis

HME realizes the evolution of $e^{-i\mathcal{N}(\rho)t}$ by sequentially inputting the target state ρ . Thus, an essential indicator for analyzing the performance of HME is the number of copies needed for realizing the desired evolution within an error up to ϵ . We present Theorem 2 below to resolve this question.

Theorem 2. (Upper bound of sample complexity). Let \mathcal{N} be an arbitrary HP map, the HME algorithm requires at most $\mathcal{O}(\epsilon^{-1} \|H\|_{\infty}^2 t^2)$ copies of sequentially inputting state ρ to ensure that $\|\mathcal{Q}_t - \mathcal{U}_t\|_{\diamond} \leq \epsilon$ holds for arbitrary ρ . Here, $H = \Lambda_{\mathcal{N}}^{\text{T}_1}$, $\mathcal{Q}_t = \mathcal{Q}_{\Delta t}^{\circ K}$ represents the realized channel with

$\mathcal{Q}_{\Delta t}(\sigma) := \text{Tr}_1 [e^{-iH\Delta t}(\rho \otimes \sigma)e^{iH\Delta t}]$ and $K = t/\Delta t$, \mathcal{U}_t is the ideal evolution channel corresponding to $e^{-iN(\rho)t}$, and $\|\cdot\|_\diamond$ denotes the diamond norm.

According to the definition of the diamond norm, Theorem 2 implies that for any state $\sigma_{\mathcal{KR}} \in \mathcal{K} \otimes \mathcal{R}$, where \mathcal{K} is the Hilbert space on which the channels \mathcal{Q}_t and \mathcal{U}_t are defined, and \mathcal{R} is a reference system with an arbitrary dimension, if the number of steps in the HME algorithm shown in Fig. 1c satisfies $K = \Theta(\epsilon^{-1} \|H\|_\infty^2 t^2)$, then

$$\|(\mathcal{U}_t - \mathcal{Q}_t) \otimes \mathcal{I}_{\mathcal{R}}(\sigma_{\mathcal{KR}})\|_1 \leq \epsilon. \tag{2}$$

This implies that the states resulting from the realized and ideal evolutions are close in terms of trace distance. Consequently, when measuring the realized post-evolution state, the measurement outcomes will be close to those obtained from the ideal post-evolution state.

In practical quantum information processing tasks, the HME algorithm is often employed in conjunction with other quantum algorithms such as quantum phase estimation or Hadamard test. These algorithms

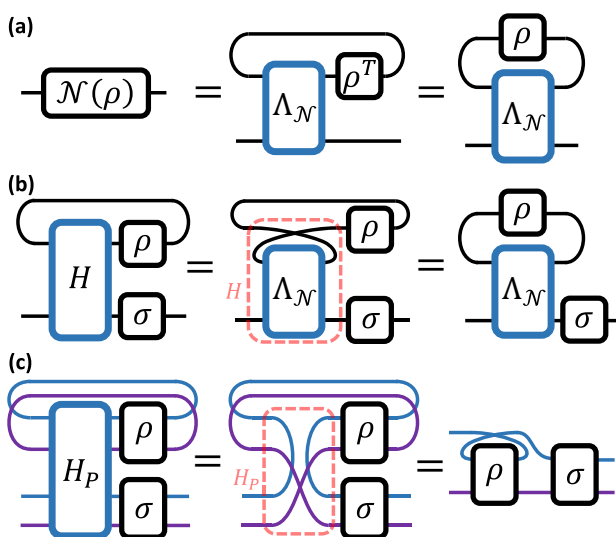


Fig. 2 | Proof of Theorem 1 using tensor network calculations. A matrix is represented using a box with left and right legs, where the left legs represent row indices and the right legs represent column indices. The connection of legs indicates the contraction between indices. In a, we illustrate the tensor network representation of the Choi matrix $\Lambda_{\mathcal{N}}$ and how it can be used to represent the action of a linear map \mathcal{N} . In b, we use the exchange of the left and right legs to represent the transposition operation. Consequently, it becomes evident that in order to ensure $\text{Tr}_1[H(\rho \otimes \sigma)] = \mathcal{N}(\rho)\sigma$, we must have $H = \Lambda_{\mathcal{N}}^T$, which is highlighted by the red dashed box. In c, we graphically demonstrate the validation of $H_P = \Phi_A^+ \otimes S_B$ for realizing the evolution of $e^{-i\rho^T A t}$, where $\rho^T A$ is the partial transpose of ρ on system A. We use blue and purple legs to represent the indices of subsystems A and B, respectively.

typically require a controlled version of the evolution $e^{-iN(\rho)t}$, as illustrated in the circuits of Fig. 4 and Fig. 5. We show that the sample complexity for exponentiating controlled $e^{-iN(\rho)t}$ evolution has the same upper bound (see “Methods”).

Corollary 1. We need at most $\mathcal{O}(\epsilon^{-1} \|H\|_\infty^2 t^2)$ copies of ρ to perform $C - e^{-iN(\rho)t} := |0\rangle\langle 0|_c \otimes \mathbb{I} + |1\rangle\langle 1|_c \otimes e^{-iN(\rho)t}$ to precision ϵ in diamond distance, where $H = \Lambda_{\mathcal{N}}^T$, and the subscript c denotes the control qubit.

Notice that $\|H\|_\infty^2$ might be unbounded for certain HP maps. Thus, an important problem arises: Is HME the optimal protocol for exponentiating certain HP maps? For an HP map, if the value of $\|H\|_\infty^2$ is large, does this mean that there exists a better algorithm, or exponentiating this HP map is fundamentally hard^{31–34}? To finger out this problem, we first consider the most general method to exponentiate a quantum state, as shown in Fig. 3a, and use Theorem 5 to show the complexity lower bound for this general method.

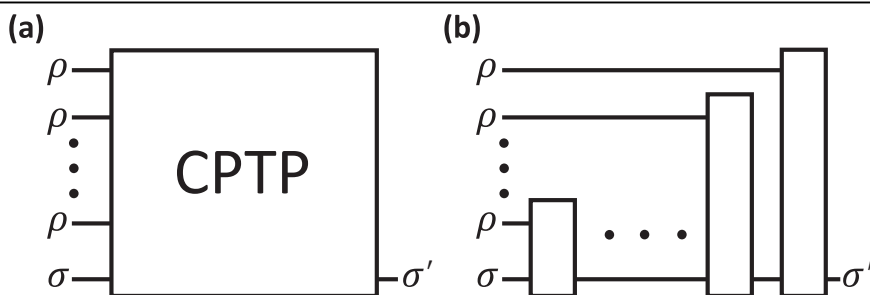
Combining Theorem 2 and Theorem 5, we find that the complexity upper bounds of HME can reach the lower bounds for exponentiating certain maps, as shown in Supplementary Material (see Supplementary Material for details of the algorithm). As demonstrated in Fig. 3b, HME is a special case for the general protocol. Therefore, we can conclude that for maps such as the inverse of local amplitude damping noise channel, the HME algorithm is the optimal method to realize $e^{-iN(\rho)t}$. It is also worth mentioning that the analysis of the upper and lower bounds for realizing $e^{-iN(\rho)t}$ also partly answers the open problem raised in ref. 35. This problem seeks to determine the sample complexity required for implementing the evolution of $e^{-if(\rho)t}$ for a given function $f(\cdot)$. Note that when only concentrating on expectation values, the optimal sampling overhead for simulating the HP map \mathcal{N} is determined by $\|\mathcal{N}\|_\diamond^2$ using the quasi-probability decomposition method^{32,36}. Further study is required to characterize the optimal sample complexity of simulating HP maps through exponentiation.

In practical situations, the performance of HME can be affected by various factors. For example, quantum devices may exhibit unpredictable and unavoidable noise, and the realization of the Hamiltonian evolution $e^{-iH\Delta t}$ may be inaccurate due to approximation errors in Hamiltonian simulation^{37,38}. Besides, the input state ρ may also be affected and deviate in each step. We analyze the robustness of HME against the input state error and the Hamiltonian error in the Supplementary Material (see Supplementary Material for details of the algorithm). Similar to the sample complexity, we show that the robustness of HME is also influenced by $\|H\|_\infty$, which could help us to find application scenarios.

Entanglement detection

Entanglement is a distinctive feature of quantum mechanics³⁹, and the detection and quantification of entanglement is of both fundamental and practical importance^{40,41}. A variety of protocols have been proposed for entanglement detection³. The positive map criteria, which include the partial transposition⁶ and reduction maps⁴², are considered to be among the most powerful entanglement detection criteria⁴³. The positive map criterion

Fig. 3 | General and sequential protocols to exponentiate a HP map. a In the most general case, joint operations are performed on multiple copies of ρ and the input state σ , which induces a channel $\sigma' = \mathcal{Q}^\rho(\sigma)$ that acts only on σ . b A sequential protocol relies on sequential operations acting on single-copies of ρ and the evolved state, where the black boxes represent different CPTP maps.



states that if $\mathcal{P}_A \otimes \mathcal{I}_B(\rho)$ is not a semi-positive matrix, then the state ρ is entangled. Here, \mathcal{P} represents the positive map being used, and A and B label the two subsystems of ρ . However, the main challenges in achieving positive map detection protocols lie in the non-CP nature of positive maps as well as the difficulty of performing spectral analysis for the exponentially large matrix $\mathcal{P}_A \otimes \mathcal{I}_B(\rho)$. These two obstacles can be overcome using the algorithms of HME and quantum phase estimation.

Combining the ability of HME to exponentiate the controlled unitary operation $e^{-i\mathcal{P}_A \otimes \mathcal{I}_B(\rho)t}$ and the quantum phase estimation algorithm, we propose an HME-based entanglement detection protocol, as illustrated in Fig. 4a. The measurements of the ancilla qubits directly provide information about the spectrum of $U = e^{-i\mathcal{P}_A \otimes \mathcal{I}_B(\rho)t}$, which is equivalent to the spectrum of $\mathcal{P}_A \otimes \mathcal{I}_B(\rho)$. If $\mathcal{P}_A \otimes \mathcal{I}_B(\rho)$ is not semi-positive, we can select σ to be a state that exhibits significant overlap with the negative subspace of $\mathcal{P}_A \otimes \mathcal{I}_B(\rho)$. Consequently, there is a significant probability of detecting the negative eigenvalues of $\mathcal{P}_A \otimes \mathcal{I}_B(\rho)$ and thus the entanglement of ρ .

This new protocol offers a systematic approach to leverage quantum resources such as quantum memory and ancilla qubits, enabling us to reduce classical repetition times and gain advantages over conventional methods. Specifically, it has been proven that if only single-copy operations are allowed, an exponential amount of resources is required for entanglement detection⁴⁵, even in the case of pure states⁴⁴. The following presents a typical example.

Fact 1. Consider a bipartite system with subsystem dimensions $d_A = d_B = \sqrt{d}$ ⁴⁴. Let ρ be a pure state, which can be either a global Haar random state ψ_{AB} or a tensor product of local Haar random pure states $\psi_A \otimes \psi_B$, each with equal probabilities. If we are limited to single-copy operations and measurements on ρ , determining whether ρ is entangled requires $\Theta(d^{1/4})$ experiments, with a success probability of at least 2/3.

Here we employ the reduction map to demonstrate the advantage of HME in entanglement detection. The reduction map R is defined as $\rho^R = \text{Tr}(\rho)\mathbb{I}_d - \rho$, where $d = d_A \times d_B$ represents the dimension of the Hilbert space of ρ . The reduction criterion involves testing whether

$$\rho^{R_A} = \mathbb{I}_{d_A} \otimes \rho_B - \rho \tag{3}$$

is semi-positive or not, where $\rho_B = \text{Tr}_A(\rho)$ denotes the reduced density matrix for subsystem B . By exponentiating the partial reduction map using HME, we find that the entanglement detection task implied in Fact 1 can be solved with a constant sample complexity using the HME-based

entanglement detection protocol, showing an exponential advantage compared with all single-copy entanglement detection protocols. Besides, the circuit for this task is shown in Fig. 4b, which requires only a single ancilla qubit.

Theorem 3. Let $H_R = \mathbb{I}_A \otimes S_B - S_{AB}$, where $\mathbb{I}_A, S_B,$ and S_{AB} stand for the identity operator acting on two copies of system A , SWAP operator acting on two copies of system B , and SWAP operator acting on two copies of the joint system AB , respectively. Choosing $t = \pi$, the circuit depicted in Fig. 4b requires at most $\mathcal{O}(1)$ copies of ρ to accomplish the task described in Fact 1 with a success probability of at least 2/3.

In addition to the constant sample complexity, the corresponding Hamiltonian $H_R = \mathbb{I}_A \otimes S_B - S_{AB}$ is 2-sparse and efficiently row computable. As a result, it can be efficiently simulated⁴⁵, leading to an overall gate complexity of our protocol that scales as $\mathcal{O}(1)$.

Entanglement quantification

Among all positive map criteria, the positive partial transposition criterion⁶ is of fundamental importance due to its strong detection capability⁴⁶, its connection to entanglement distillation⁹, and its concise mathematical formulation. The positive partial transposition criterion states that if the target state ρ is separable, then the matrix ρ^{T_A} has no negative eigenvalues, where T_A denotes the partial transposition map on a subsystem A . The entanglement negativity serves as an entanglement measure by quantifying the violation of the positive partial transposition criterion,

$$N(\rho) = \frac{\|\rho^{T_A}\|_1 - 1}{2}, \tag{4}$$

which equals the sum of the absolute values of all negative eigenvalues of ρ^{T_A} . As a widely used quantifier for mix-state entanglement, negativity plays an indispensable role in theoretical physics^{8,47,48}.

However, due to the non-CP nature of the transposition map and the highly nonlinear behavior of negativity, there is still no efficient protocol for unbiasedly estimating negativity. Some approaches, such as directly measuring the spectral values of ρ^{T_A} ^{21,49}, require joint operations on exponentially many copies of quantum states. Tomography-based protocols estimate negativity by reconstructing the density matrix, which requires a large sample complexity and significant classical computational

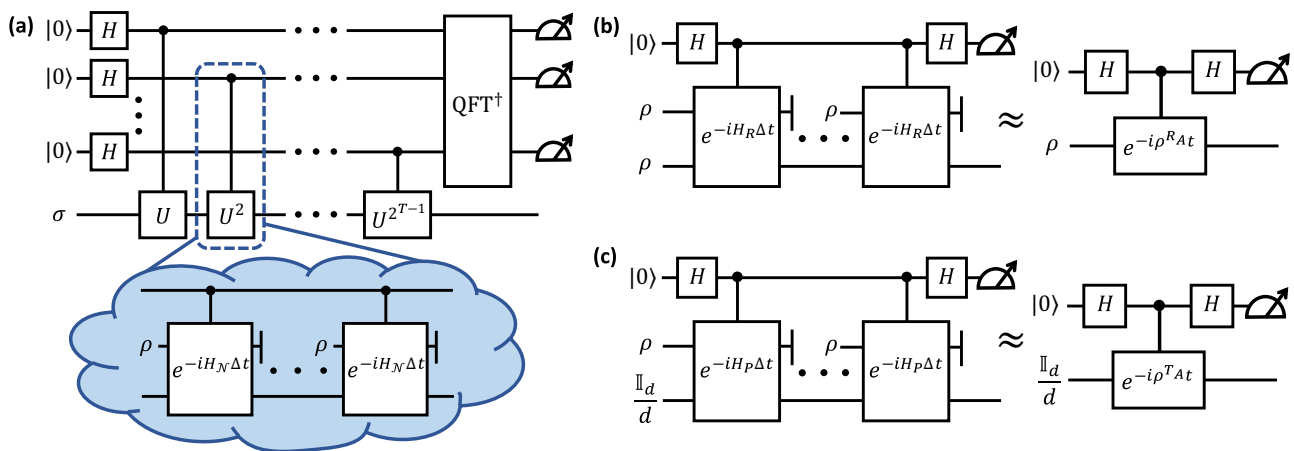
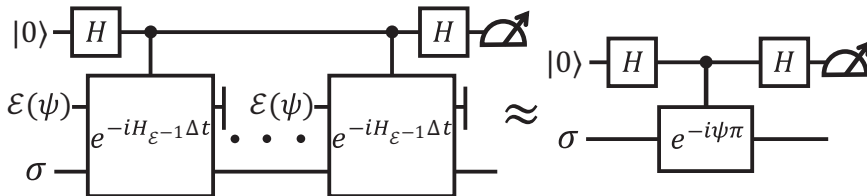


Fig. 4 | Application of HME in entanglement detection and quantification. **a** Represents the circuit of the HME-based entanglement detection protocol, which is constructed by combining the HME and quantum phase estimation algorithms. The quantum phase estimation consists of the input state σ , T ancilla qubits, controlled unitary operations, inverse quantum Fourier transformation, and final measurements on the ancilla qubits. The controlled unitary evolutions are approximately realized by HME, where H_N is the Hamiltonian for exponentiating

$N = \mathcal{P}_A \otimes \mathcal{I}_B$. **b** is a special case of **a** where only one ancilla qubit remains, the inverse quantum Fourier transformation is reduced to the Hadamard gate, and H_R is the Hamiltonian for exponentiating the partial reduction map. The evolved state and sequentially inputted states are set to the target state of the entanglement detection task. **c** is the circuit for estimating entanglement negativity. Compared with **b**, we change the evolved state to the maximally mixed state and the Hamiltonian to H_P .

Fig. 5 | The circuit of our noiseless state recovery protocol. The Hamiltonian is set to be $H_{\mathcal{E}^{-1}} = \Lambda_{\mathcal{E}^{-1}}^{\dagger}$, the partial transposition of the Choi matrix of the inverse map \mathcal{E}^{-1} . The evolved state σ serves as a guiding state which needs to have a high fidelity with the noiseless state ψ .



resources^{50,51}. Other attempts primarily utilize the moments of the partially transposed density matrix to infer properties of negativity^{10,52}, rather than providing an unbiased estimation.

HME can also alleviate the difficulties in measuring negativity. Firstly, as illustrated in Fig. 2c, HME can realize the evolution of $e^{-i\rho^{T_A}t}$ by setting the evolution Hamiltonian to $H_p = \Phi_A^+ \otimes S_B$. Secondly, as $e^{-i\rho^{T_A}t}$ is a nonlinear function of ρ^{T_A} , HME enables the measurement of certain nonlinear quantities including entanglement negativity^{53,54}. Specifically, we can combine the HME algorithm and Hadamard test algorithm and use the circuit shown in Fig. 4c to estimate $\text{tr}[\cos(\rho^{T_A}t)]$ in different values of t . According to Fourier decomposition, we can use these quantities to construct an unbiased estimation of entanglement negativity. We show details of this estimation protocol in Methods.

Theorem 4. One needs an expected number of $\tilde{O}(\log(\delta^{-1})\epsilon^{-3}d^2d_A\|\rho^{T_A}\|_1)$ copies of ρ to ensure $|\hat{N}(\rho) - N(\rho)| \leq \epsilon$ with a probability of at least $1 - \delta$. Here, the \tilde{O} notation suppresses logarithmic expressions for d and ϵ , d_A stands for the dimension of subsystem A .

We leave the technical proof of Theorem 4 in the Supplementary Material (see Supplementary Material for details of the algorithm). Due to the property of entanglement negativity, $\|\rho^{T_A}\|_1 = \|\rho^{T_B}\|_1$, we can always assume $d_A \leq d_B$. As $\|\rho^{T_A}\|_1 \leq d_A$, the worst case sample complexity is at most $\tilde{O}(\epsilon^{-3}d^3)$. Compared to the tomography-based negativity estimation protocol, our protocol has advantages in both quantum and classical resource consumption. Due to the fact that negativity can be exponentially large, the tomography-based protocol requires $\theta(\epsilon^{-2}d^4)$ repetition times to accurately estimate negativity⁵¹. Thus, HME showcases polynomial improvement in sample complexity. Additionally, the tomography-based protocol requires performing spectral decomposition of the reconstructed density matrix, which also consumes exponential classical resources for computation and memory. Since the HME-based protocol relies on directly accessible quantities, we can save these classical resources.

Quantum noiseless state recovery

Noises in quantum circuits act as a significant obstacle to implementing quantum algorithms^{55,56}. Researchers have dedicated significant efforts to handling quantum noises, resulting in various protocols that can be categorized into two main types: quantum error correction and mitigation. By encoding the target state into a larger Hilbert space, quantum error correction protects the target state against a large variety of errors⁵⁷⁻⁶⁰. When the physical noise rate is below a certain threshold⁶¹, quantum error correction can suppress the logical error rate to an arbitrarily small value by consuming a large number of ancilla qubits⁶². Quantum error mitigation^{4,5} focuses on a simpler task of recovering the noiseless expectation value using multiple noisy states. Some error mitigation protocols are tailored to handle specific types of noises, such as virtual distillation^{63,64} for incoherent errors and subspace expansion for coherent errors⁶⁵. Some protocols are designed to handle general forms of noises, such as probabilistic error cancellation¹²⁻¹⁴, which is one of the leading error mitigation approaches. Quantum error mitigation typically requires an exponential number of experiments to accurately estimate the noiseless expectation value^{66,67}.

Building upon HME, we propose a new protocol to handle quantum noises, which is named quantum noiseless state recovery. We consider a

similar setting as quantum error mitigation where many noisy states are provided. Suppose the ideal noiseless state ψ is generated by an ideal noiseless circuit, $\psi = \mathcal{U}(|0\rangle\langle 0|)$, while the existence of noise will change it to $\mathcal{E}(\psi) = \mathcal{E} \circ \mathcal{U}(|0\rangle\langle 0|)$. Note that \mathcal{E}^{-1} is always HP when it exists³¹, thus the exponentiation of \mathcal{E}^{-1} becomes possible with HME. By sequentially inputting multiple copies of $\mathcal{E}(\psi)$ into the circuit depicted in Fig. 1c and choosing an appropriate Hamiltonian, we can approximately realize the evolution of

$$e^{-i\mathcal{E}^{-1} \circ \mathcal{E}(\psi)t} = e^{-i\psi t} \tag{5}$$

with arbitrary accuracy.

It is evident that $e^{-i\psi t}$ has only one nontrivial eigenvalue, e^{-it} , with the corresponding eigenstate $|\psi\rangle$. Setting $t = \pi$, a simple circuit shown in Fig. 5 can be used to prepare the noiseless state ψ and thus serves as the circuit for quantum noiseless state recovery. The correctness of our protocol is ensured by the following proposition:

Proposition 1. When measuring the ancilla qubit in the ideal circuit depicted on the right side of Fig. 5, the outcome $|1\rangle$ occurs with a probability of $\langle \psi | \sigma | \psi \rangle$. If the outcome $|1\rangle$ is observed, σ will evolve into the desired noiseless pure state $|\psi\rangle$.

Note that in a practical situation where the noise rate is relatively small, one can choose the noisy state $\mathcal{E}(\psi)$ as the evolved state σ to increase the success probability. Considering the approximation error of the HME algorithm and the success rate of post-selection, we derived the performance of our noiseless state recovery protocol, shown in Theorem 6 in Methods.

Quantum noiseless state recovery faces practical challenges of requiring precise knowledge of the noise channel, the calculation of the inverse map, and efficient methods for realizing controlled Hamiltonian evolution. However, its fundamental differences from conventional error management protocols offer inspiration for alternative error management protocols and warrant a deeper understanding of its characteristics. Notably, quantum noiseless state recovery is the first protocol that can recover the noiseless quantum state without any encoding operation. Specifically, our protocol starts from states that have already been influenced by noises, like quantum error mitigation. However, what sets our protocol apart is its capacity to recover noiseless quantum states. Such ability brings advantages in various applications⁵, such as quantum storage and quantum communication, where noise-free states are desired. It is also crucial in practical scenarios like the Shor algorithm and quantum key distribution, where noiseless states enable obtaining single-shot measurement results instead of just expectation values. Compared to quantum error correction, our protocol requires fewer ancilla qubits and does not necessitate access to the noiseless state at the beginning. A more comprehensive comparison can be found in the Supplementary Material (see Supplementary Material for details of the algorithm).

Discussion

The Hermitian-preserving map exponentiation algorithm relies on quantum memory, ancillary systems, joint operations, and the ability to reset states. In all three applications discussed in the main text, the HME algorithm requires doubling the system size and performing joint evolution. Without these resources, methods such as quasi-probability decomposition

can still simulate non-CP maps when only focusing on expectation values^{32,36}, offering a more practical approach for applications on near-term devices. Based on these resources, the advantages of HME manifest in three aspects. Firstly, quantum memory is known to provide exponential speedups in certain tasks such as state discrimination and property testing⁶⁸. Consequently, HME exhibits exponential speedups compared to single-copy protocols, as demonstrated in tasks of entanglement detection and quantification. Secondly, by employing ancilla qubits, HME enables the transformation of incoherent operations into coherent ones, thereby realizing tasks that are infeasible for incoherent operations. An important example is the comparison between the noiseless state recovery protocol and quantum error mitigation. Due to the limitation of single-copy operations, quantum error mitigation can only recover the noiseless expectation values. While using HME, it becomes possible to recover the noiseless state from noisy states, thereby facilitating single-shot measurements and tasks such as quantum storage. Additionally, HME offers a means to utilize quantum resources to replace classical resources, especially in state benchmarking protocols. Leveraging state-resetting operations, HME extracts information from multiple copies of states, reducing the classical resources for estimating some state properties. A direct example is the negativity estimation where HME exponentially reduces the requirements for classical computation and memory compared to tomography-based methods.

As HP maps are ubiquitous in quantum information science, HME has potential applications in many other fields. An intriguing observation is that when measuring an observable, $\text{Tr}(O\rho)$ is also a HP map that acts on ρ . Thus, by exponentiating $\mathcal{N}_O(\rho) = \text{Tr}(O\rho)|1\rangle\langle 1|$, HME enables the encoding of expectation values into relative phases of reference states. In addition to the expectation value measurement, such HME-based phase encoding operation may also have applications in tasks such as gradient estimation^{69,70}. In many quantum information tasks, completely positive while not trace-preserving maps $\mathcal{N}(\rho) = P\rho P^\dagger$ play important roles. For example, in the task of the linear combination of unitaries, the matrix P is chosen as the sum of many unitaries, allowing for producing a target pure state or realizing a desired Hamiltonian evolution⁷¹. In quantum imaginary time evolution⁷²⁻⁷⁴, P is set as $e^{-\beta H}$, where β represents the inverse temperature and H is a Hamiltonian. By increasing β , one can prepare a pure state that approximates the ground state of H to arbitrary precision. By exponentiating $\mathcal{N}(\rho) = P\rho P^\dagger$ with HME, we can use a circuit similar to Fig. 5 to prepare the pure state which is the target of the linear combination of unitaries or quantum imaginary time evolution. We emphasize that, when exploring new applications of HME, it is essential to ensure that both the sample complexity and gate complexity remain manageable.

As discussed, a major application of HME is quantum state learning, which includes observable measurement, entanglement detection, and negativity estimation. Thus, comparing HME with one commonly used quantum state learning protocol, classical shadow⁷⁵ is inspiring. Conducted in a “measure first, ask questions later”⁷⁶ manner, the quantum experiments stage of classical shadow does not utilize the information of the task. HME also provides a systematic scheme for quantum state learning tasks by adjusting the HP map \mathcal{N} . Thus, a key difference between HME and classical shadow is that the quantum experiment of HME facilitates the information of the task to determine \mathcal{N} . Besides, classical shadow only relies on incoherent operations and classical post-processing, while HME utilizes quantum memories and coherent operations. These differences bring advantages for HME, such as the exponential speedups in entanglement detection and the classical computational resources saving in negativity estimation. Nonetheless, the construction of classical shadow and HME share many similar techniques, suggesting an important future direction in combining these two protocols.

As a building block for quantum algorithms, the HME algorithm holds the potential for further improvement. One possible direction is to combine HME with algorithms such as amplitude amplification, which could enhance the performance of tasks discussed in this work, including noiseless state recovery. Moreover, by replacing the Hamiltonian evolution in the HME circuit with non-Hermitian evolution, HME can even circumvent the

Hermitian preservation requirement and showcases potential advantages for a wider range of tasks involving maps that are not HP⁷⁷.

It is worth noting that the capability to simulate non-CP maps is not exclusive to the HME algorithm. Notably, block encoding and quantum singular value transformation is usually adopted to simulate complex evolution of quantum states^{78,79}. Thus, it is an important future direction to explore how to use these techniques to simulate non-CP maps, which can potentially help us to break the limitation of linearity. However, there are some difficulties. Firstly, block-encoding requires an oracle which can prepare the purification of ρ , whereas HME solely requires ρ itself. Such oracle is infeasible for many practical scenarios, including entanglement detection and quantum error mitigation discussed previously. Thus, it is crucial to find suitable applications for block-encoding. Besides, the original quantum singular value transformation is only capable of performing maps that act on the singular values of the encoded matrix ρ . Performing linear maps like partial transpose requires additional effort.

Methods

Below, we present the proof of the theorems in the main text and describe the details of the negativity estimation protocol.

Proof of Theorem 1

Substituting the Taylor expansion $e^{-iH\Delta t} = \mathbb{I} - iH\Delta t + \mathcal{O}(\Delta t^2)$ into Eq. (1), the left-hand side becomes

$$\sigma - i\Delta t \text{Tr}_1([H, \rho \otimes \sigma]) + \mathcal{O}(\Delta t^2). \quad (6)$$

According to the Choi-Jamiołkowski isomorphism⁸⁰, the resulting state of a map \mathcal{N} can be represented using the Choi matrix $\Lambda_{\mathcal{N}}$, as $\mathcal{N}(\rho) = \text{Tr}_1(\Lambda_{\mathcal{N}}(\rho^T \otimes \mathbb{I}))$. Following this definition, we can rewrite the coefficient of the first-order term in Eq. (6) as

$$\text{Tr}_1([H, \rho \otimes \sigma]) = [\text{Tr}_1(\Lambda_{\mathcal{N}}(\rho^T \otimes \mathbb{I}), \sigma), \quad (7)$$

which by definition equals $[\mathcal{N}(\rho), \sigma]$. It can be verified that $[\mathcal{N}(\rho), \sigma]$ is also the coefficient of the first-order term of $e^{-i\mathcal{N}(\rho)\Delta t} \sigma e^{i\mathcal{N}(\rho)\Delta t}$. To provide a clearer derivation, we present a graphical demonstration of this proof based on tensor network representation in Fig. 2b.

Since $H = \Lambda_{\mathcal{N}}^{\dagger}$ and H is the Hamiltonian of the composite system, $\Lambda_{\mathcal{N}}$ must be a Hermitian operator. Therefore, the only restriction on \mathcal{N} is that it should be HP.

Proof of Corollary 1

Based on the equality $C - e^{-i\mathcal{N}(\rho)t} = e^{-i|1\rangle\langle 1|_c \otimes \mathcal{N}(\rho)t}$, we can define a new HP map $\mathcal{N}'(\rho) = |1\rangle\langle 1|_c \otimes \mathcal{N}(\rho)$. Therefore, in the circuit of HME depicted in Fig. 1c, we can add a control qubit and regard the control qubit together with σ as the evolved state of a new HME circuit, with a new Hamiltonian $H' = |1\rangle\langle 1|_c \otimes H$. Since $|1\rangle\langle 1|_c \otimes H$ has the same operator norm as H , according to Theorem 2, we get the desired result. Note that based on the same reasoning, Corollary 1 can be straightforwardly extended to scenarios where the number of control qubits is greater than one.

Proof sketch of Theorem 2

We sketch the core idea for proving Theorem 2 in this section and leave the complete proof to the Supplementary Material (see Supplementary Material for details of the algorithm). We divide the ideal evolution channel \mathcal{U}_t into K slices $\mathcal{U}_t = \mathcal{U}_{\Delta t}^{\circ K}$, where $\mathcal{U}_{\Delta t}$ refers to the unitary evolution of $e^{-i\mathcal{N}(\rho)\Delta t}$. Intuitively, the closeness of $\mathcal{Q}_{\Delta t}$ and $\mathcal{U}_{\Delta t}$ ensures the closeness of \mathcal{Q}_t and \mathcal{U}_t . According to the subadditivity property of the diamond distance, we obtain

$$\|\mathcal{Q}_t - \mathcal{U}_t\|_{\diamond} \leq K \|\mathcal{Q}_{\Delta t} - \mathcal{U}_{\Delta t}\|_{\diamond}, \quad (8)$$

which implies that the error accumulates linearly during the sequential operations. By employing certain matrix inequalities, we arrive at

$$\|U_{\Delta t} - Q_{\Delta t}\|_{\diamond} \leq \mathcal{O}(\|H\|_{\infty}^2 \Delta t^2) = \mathcal{O}(\|H\|_{\infty}^2 t^2 / K^2). \quad (9)$$

Hence, the total diamond distance scales as $\mathcal{O}(\|H\|_{\infty}^2 t^2 / K)$. Therefore, to ensure that the total diamond distance is less than ϵ , the number of steps K , or equivalently, the number of copies of ρ , needs to be at most $\mathcal{O}(\epsilon^{-1} \|H\|_{\infty}^2 t^2)$.

Sample complexity lower bound

Theorem 5. (Lower bound of sample complexity). Let $\mathcal{N} \in T(\mathcal{H}, \mathcal{K})$ be a HP map and set $0 < \epsilon \leq 1/6$, and $t \geq \frac{15\pi\epsilon}{4R_*}$. The minimum number of ρ needed to realize the evolution of $e^{-i\mathcal{N}(\rho)t}$ with ϵ accuracy in diamond distance satisfies

$$f_{\mathcal{N}}(\epsilon, t) \geq (\epsilon^{-1} R_*^2 t^2), \quad (10)$$

where $R_* := \max A \in \mathcal{F} R[\mathcal{N}(A)]$. $R[\cdot] = \lambda_{\max}(\cdot) - \lambda_{\min}(\cdot)$ denotes the spectral gap defined as the difference between the largest and the smallest eigenvalues of the processed matrix. The feasible region \mathcal{F} is defined as

$$\mathcal{F} = \{A \in L(\mathcal{H}) : A^\dagger = A, \text{Tr}(A) = 0, \|A\|_1 = 1, [\mathcal{N}(A^+), \mathcal{N}(A^-)] = 0\}, \quad (11)$$

where A^+ and A^- are the positive and negative parts of A . The key principle for proving this theorem is the Holevo-Helstrom theorem^{2,81,82}, which deals with the discriminations of states and channels. According to this theorem, the optimal success probability for discriminating two different states is $\frac{1}{2} + \frac{1}{4} \|\rho_0 - \rho_1\|_1$, and for discriminating two different channels is $\frac{1}{2} + \frac{1}{4} \|Q_0 - Q_1\|_{\diamond}$. When allowed to perform joint operations on K copies of the unknown state ρ , discrimination becomes easier with more copies, as $\|\rho_0^{\otimes K} - \rho_1^{\otimes K}\|_1$ increases with K .

For a given HP map \mathcal{N} , there may exist two states ρ_0 and ρ_1 such that the trace distance between them can be much lower than the diamond distance between the two ideal evolution channels, $\|\rho_0 - \rho_1\|_1 \ll \| [e^{-i\mathcal{N}(\rho_0)t}] - [e^{-i\mathcal{N}(\rho_1)t}] \|_{\diamond}$, for some t . According to the Holevo-Helstrom theorem, this implies that the discrimination of these two states is more challenging compared to distinguishing the ideal evolution channels. Thus, if the induced channel of Fig. 3a, denoted as Q^{ρ} , can approximate the ideal channel $[e^{-i\mathcal{N}(\rho)t}]$ for all states ρ , the discrimination between the channels Q^{ρ_0} and Q^{ρ_1} will also be easier than that of ρ_1 and ρ_2 . Since the CPTP map used in Fig. 3a is independent of the input state ρ , the discrimination between the channels Q^{ρ_0} and Q^{ρ_1} guarantees the discrimination between the states ρ_0 and ρ_1 . This implies that there exists a fundamental lower bound on the number of copies for ρ required to realize Q^{ρ} , given by $\|\rho_0^{\otimes K} - \rho_1^{\otimes K}\|_1 \geq \|Q^{\rho_0} - Q^{\rho_1}\|_{\diamond}$, which serves as the key equation for deriving the lower bound on K . The choices of ρ_0 and ρ_1 are related to the feasible region \mathcal{F} defined in Eq. (11).

Proof sketch of Theorem 3

The constant sample complexity given in Theorem 3 can be explained based on the following reasons. First, since $\|H_R\|_{\infty} = 2$, which remains constant as the system size grows, the cost of exponentiating the controlled- $e^{-ip^{R_A}t}$ evolution does not scale with system dimension, as indicated by Corollary 1. Second, as shown in the right-hand side of Fig. 4b, a single ancilla qubit and controlled unitary evolution is sufficient for the quantum phase estimation algorithm. When $\rho = \psi_A \otimes \psi_B$, the lowest eigenvalue of $\rho^{R_A} = \mathbb{I}_{d_A} \otimes \psi_B - \psi_A \otimes \psi_B$ is zero. On the other hand, when $\rho = \psi_{AB}$ is a global random pure state, then the lowest eigenvalue of $\rho^{R_A} = \mathbb{I}_{d_A} \otimes \rho_B - \psi_{AB} \sim \frac{1}{d_B} \mathbb{I}_d - \psi_{AB}$ is

approximately -1 , especially for large d . Therefore, by setting $t = \pi$, the eigenvalues of $e^{-i(\psi_{AB})^{R_A}t}$ and $e^{-i(\psi_A \otimes \psi_B)^{R_A}t}$ corresponding to the lowest eigenvalues of $(\psi_{AB})^{R_A}$ and $(\psi_A \otimes \psi_B)^{R_A}$ are approximately $e^{i\pi}$ and e^0 , respectively. As the binary representations of $\pi/2\pi$ and $0/2\pi$ are 0.1 and 0, a single ancilla qubit, which is equivalent to a single controlled unitary operation in quantum phase estimation, is sufficient for telling these two different eigenvalues. Finally, one round of the experiment is sufficient. This is because ρ itself has a significant overlap with the eigenspace corresponding to the lowest eigenvalue of ρ^{R_A} in both cases. Therefore, by setting the evolved state σ to be ρ , as depicted in Fig. 4b, one round of experiment can detect the entanglement with a significantly high probability.

The complete proof can be found in the Supplementary Material (see Supplementary Material for details of the algorithm).

Negativity estimation protocol

Below, we present our negativity estimation protocol, inspired by the Hadamard-test-like circuit in ref. 30, as depicted in Fig. 4c. This type of circuit was originally designed for estimating the trace of a unitary. Following a similar approach, by setting the evolved state as the maximally mixed state and performing the controlled- $e^{-ip^{T_A}t}$ operation on the ancilla and evolved states using HME, we can estimate quantities like $\text{Tr}[\cos(\rho^{T_A}t)]$ or $\text{Tr}[\sin(\rho^{T_A}t)]$ depending on the measurement basis of the ancilla qubit. For instance, measuring the expectation value of the Pauli-X operator on the ancilla qubit would yield

$$\begin{aligned} & \text{Tr}\left[(X \otimes \mathbb{I}_d)C - e^{-ip^{T_A}t} \left(|+\rangle\langle+| \otimes \frac{\mathbb{I}_d}{d}\right)C - e^{ip^{T_A}t}\right] \\ &= \frac{1}{2d} \text{Tr}\left[e^{-ip^{T_A}t} + e^{ip^{T_A}t}\right] = \frac{1}{d} \text{Tr}\left[\cos(\rho^{T_A}t)\right], \end{aligned} \quad (12)$$

where $C = e^{-\rho^{T_A}t} = |0\rangle\langle 0| \otimes \mathbb{I}_d + |1\rangle\langle 1| \otimes e^{-ip^{T_A}t}$. The measurement of $\text{Tr}[\cos(\rho^{T_A}t)]$ with different values of t enables us to estimate the negativity, which can be expressed as a convergent Fourier expansion,

$$\|\rho^{T_A}\|_1 = \frac{\pi}{2}d - \sum_{l=1}^{\infty} \frac{4}{\pi(2l-1)^2} \text{Tr}[\cos((2l-1)\rho^{T_A})]. \quad (13)$$

In particular, this HME-based negativity estimation algorithm repeats the following procedures for a total of M times:

1. Randomly sample an integer l with a probability distribution according to the coefficients of Eq. (13).
2. Run the circuit of Fig. 4c for one shot with evolution time $t = (2l-1)$ and $K(l)$ copies of inputting states ρ to produce an estimation of $\text{Tr}[\cos((2l-1)\rho^{T_A})]$ using the measurement result of the ancilla qubit.

By taking the median of means of these sequentially generated estimations, we can get the final estimation of entanglement negativity. The details of this algorithm and sample complexity analysis can be found in the Supplementary Material (see Supplementary Material for details of the algorithm).

Proof of Proposition 1

Observe that $e^{-i\psi\pi} = \mathbb{I} - 2\psi$, when the controlled- $e^{-i\psi\pi}$ gate is applied to the ancilla qubit and the evolved state σ , the whole state will evolve into

$$= \frac{1}{2} \begin{bmatrix} \sigma & \sigma - 2\psi\sigma \\ \sigma - 2\psi\sigma & \sigma - 2\psi\sigma - 2\psi\sigma + 4\psi\sigma\psi \end{bmatrix}, \quad (14)$$

whose row and column indices labeling the matrix blocks correspond to the indices of the ancilla qubit. When the measurement outcome of the ancilla qubit is $|1\rangle$, which corresponds to measuring $|-\rangle \otimes \mathbb{I}_d$ on Σ , the resulting

state will become

$$\begin{aligned} & \text{Tr}_c \left(\frac{(|-\rangle\langle -| \otimes I_d)(|-\rangle\langle -| \otimes I_d)}{\text{Tr}[(|-\rangle\langle -| \otimes I_d)]} \right) \\ &= \frac{1}{\langle \psi | \sigma | \psi \rangle} \text{Tr}_c \left(\frac{1}{2} \begin{bmatrix} \psi \sigma \psi & -\psi \sigma \psi \\ -\psi \sigma \psi & \psi \sigma \psi \end{bmatrix} \right) = \psi, \end{aligned} \quad (15)$$

where Tr_c denotes tracing out the control qubit, and $\langle \psi | \sigma | \psi \rangle$ is the probability for getting the outcome $|1\rangle$.

Sample complexity of quantum noiseless state recovery

The sample complexity of quantum noiseless state recovery is mainly influenced by two factors. First, the realization of the controlled- $e^{-i\psi\pi}$ evolution requires multiple input states $\mathcal{E}(\psi)$, the number of which is upper bounded by $\mathcal{O}(\epsilon^{-1} \|H_{\mathcal{E}^{-1}}\|_{\infty}^2 \pi^2) = \mathcal{O}(\epsilon^{-1} \|H_{\mathcal{E}^{-1}}\|_{\infty}^2)$, as predicted in Corollary 1. Yet, after this evolution, one performs measurements and post-selection to prepare the target state. This post-selection amplifies a block in the whole state Σ by $\langle \psi | \sigma | \psi \rangle^{-1}$ times. Intuitively, to keep the deviation of the prepared state from the ideal state smaller than ϵ , one needs to realize the controlled- $e^{-i\psi\pi}$ evolution with an accuracy of $\langle \psi | \sigma | \psi \rangle \epsilon$, which increases the sample complexity by a factor of $\langle \psi | \sigma | \psi \rangle^{-1}$. Second, only when the measurement outcome of the ancilla qubit is $|1\rangle$, the resultant state will be ψ . Thus, on average, a number of $\langle \psi | \sigma | \psi \rangle^{-1}$ experiments are needed to obtain one successful experiment. Considering all these factors, we can arrive at the overall sample complexity.

Theorem 6. Let \mathcal{E} be an invertible noise map. Denote $H_{\mathcal{E}^{-1}} := \Lambda_{\mathcal{E}^{-1}}^{\text{T}_1}$ as the Hamiltonian to realize \mathcal{E}^{-1} in HME, and let $F := \langle \psi | \sigma | \psi \rangle$ be the fidelity between $|\psi\rangle\langle\psi|$ and σ . Then we need at most $\mathcal{O}(\log(\delta^{-1})\epsilon^{-1}F^{-2}\|H_{\mathcal{E}^{-1}}\|_{\infty}^2)$ copies of $\mathcal{E}(|\psi\rangle\langle\psi|)$ to approximately produce $|\psi\rangle\langle\psi|$ within trace distance ϵ and a success probability at least $1 - \delta$.

Data availability

The data that support this study are available upon reasonable request.

Code availability

The codes that support this study are available upon reasonable request.

Received: 26 December 2023; Accepted: 16 December 2024;

Published online: 30 December 2024

References

- Nielsen, M. A. & Chuang, I. L. *Quantum Computation and Quantum Information: 10th Anniversary Edition* (Cambridge University Press, 2010).
- Watrous, J. *The Theory of Quantum Information* (Cambridge University Press, Cambridge, 2018).
- Gühne, O. & Tóth, G. Entanglement detection. *Phys. Rep.* **474**, 1 (2009).
- Endo, S., Cai, Z., Benjamin, S. C. & Yuan, X. Hybrid quantum-classical algorithms and quantum error mitigation. *J. Phys. Soc. Jpn.* **90**, 032001 (2021).
- Cai, Z. et al. Quantum error mitigation, <https://arxiv.org/abs/2210.00921> (2022).
- Peres, A. Separability criterion for density matrices. *Phys. Rev. Lett.* **77**, 1413 (1996).
- Elben, A. et al. Mixed-state entanglement from local randomized measurements. *Phys. Rev. Lett.* **125**, 200501 (2020).
- Vidal, G. & Werner, R. F. Computable measure of entanglement. *Phys. Rev. A* **65**, 032314 (2002).
- Horodecki, M., Horodecki, P. & Horodecki, R. Mixed-state entanglement and distillation: Is there a “bound” entanglement in nature? *Phys. Rev. Lett.* **80**, 5239 (1998).
- Gray, J., Banchi, L., Bayat, A. & Bose, S. Machine-learning-assisted many-body entanglement measurement. *Phys. Rev. Lett.* **121**, 150503 (2018).
- Zhou, Y., Zeng, P. & Liu, Z. Single-copies estimation of entanglement negativity. *Phys. Rev. Lett.* **125**, 200502 (2020).
- Temme, K., Bravyi, S. & Gambetta, J. M. Error mitigation for short-depth quantum circuits. *Phys. Rev. Lett.* **119**, 180509 (2017).
- Endo, S., Benjamin, S. C. & Li, Y. Practical quantum error mitigation for near-future applications. *Phys. Rev. X* **8**, 031027 (2018).
- Guo, Y. & Yang, S. Quantum error mitigation via matrix product operators. *PRX Quantum* **3**, 040313 (2022).
- Cao, N., Fitzsimmons, M., Mann, Z., Pereira, R. & Laflamme, R. Quantum maps between cptp and hptp. Preprint at <https://arxiv.org/abs/2308.01894> (2023).
- Pechukas, P. Reduced dynamics need not be completely positive. *Phys. Rev. Lett.* **73**, 1060 (1994).
- Salgado, D., Sánchez-Gómez, J. L. & Ferrero, M. Evolution of any finite open quantum system always admits a kraus-type representation, although it is not always completely positive. *Phys. Rev. A* **70**, 054102 (2004).
- Shaji, A. & Sudarshan, E. Who’s afraid of not completely positive maps? *Phys. Lett. A* **341**, 48 (2005).
- Carteret, H. A., Terno, D. R. & Życzkowski, K. Dynamics beyond completely positive maps: Some properties and applications. *Phys. Rev. A* **77**, 042113 (2008).
- Dominy, J. M. & Lidar, D. A. Beyond complete positivity. *Quantum Inf. Process.* **15**, 1349 (2016).
- Horodecki, P. & Ekert, A. Method for direct detection of quantum entanglement. *Phys. Rev. Lett.* **89**, 127902 (2002).
- Korbicz, J. K., Almeida, M. L., Bae, J., Lewenstein, M. & Acín, A. Structural approximations to positive maps and entanglement-breaking channels. *Phys. Rev. A* **78**, 062105 (2008).
- Petz, D. Sufficient subalgebras and the relative entropy of states of a von neumann algebra. *Commun. Math. Phys.* **105**, 123 (1986).
- Gilyén, A., Lloyd, S., Marvian, I., Quek, Y. & Wilde, M. M. Quantum algorithm for petz recovery channels and pretty good measurements. *Phys. Rev. Lett.* **128**, 220502 (2022).
- Dong, Q., Quintino, M. T., Soeda, A. & Murao, M. Implementing positive maps with multiple copies of an input state. *Phys. Rev. A* **99**, 052352 (2019).
- Lloyd, S., Mohseni, M. & Rebentrost, P. Quantum principal component analysis. *Nat. Phys.* **10**, 631 (2014).
- Kjaergaard, M. et al. Demonstration of density matrix exponentiation using a superconducting quantum processor. *Phys. Rev. X* **12**, 011005 (2022).
- Huang, H.-Y. et al. Quantum advantage in learning from experiments. *Science* **376**, 1182 (2022).
- Kitaev, A. Y. Quantum measurements and the abelian stabilizer problem, <https://arxiv.org/abs/quant-ph/9511026> (1995).
- Knill, E. & Laflamme, R. Power of one bit of quantum information. *Phys. Rev. Lett.* **81**, 5672 (1998).
- Jiang, J., Wang, K. & Wang, X. Physical Implementability of Linear Maps and Its Application in Error Mitigation. *Quantum* **5**, 600 (2021).
- Regula, B., Takagi, R. & Gu, M. Operational applications of the diamond norm and related measures in quantifying the non-physicality of quantum maps. *Quantum* **5**, 522 (2021).
- Kimmel, S., Lin, C. Y.-Y., Low, G. H., Ozols, M. & Yoder, T. J. Hamiltonian simulation with optimal sample complexity. *npj Quantum Inf.* **3**, 13 (2017).
- Grasa, P. R. Enhancing the lloyd-mohseni-rebentrost algorithm for information loading. Master’s thesis https://nquirephysics.com/wp-content/uploads/2022/09/TFM-Pablo_Rodriguez_Grasa.pdf (2022).
- Anshu, A. & Arunachalam, S. A survey on the complexity of learning quantum states. *Nat. Rev. Phys.* **6**, 59 (2024).

36. Zhao, X., Zhang, L., Zhao, B. & Wang, X. Power of quantum measurement in simulating unphysical operations. Preprint at <https://arxiv.org/abs/2309.09963> (2023).
37. Suzuki, M. Fractal decomposition of exponential operators with applications to many-body theories and monte carlo simulations. *Phys. Lett. A* **146**, 319 (1990).
38. Suzuki, M. General theory of fractal path integrals with applications to many body theories and statistical physics. *J. Math. Phys.* **32**, 400 (1991).
39. Horodecki, R., Horodecki, P., Horodecki, M. & Horodecki, K. Quantum entanglement. *Rev. Mod. Phys.* **81**, 865 (2009).
40. Pan, J.-W. et al. Multiphoton entanglement and interferometry. *Rev. Mod. Phys.* **84**, 777 (2012).
41. Calabrese, P. & Cardy, J. Entanglement entropy and quantum field theory. *J. Stat. Mech. Theory Exp.* **2004**, P06002 (2004).
42. Horodecki, M. & Horodecki, P. Reduction criterion of separability and limits for a class of distillation protocols. *Phys. Rev. A* **59**, 4206 (1999).
43. Liu, P., Liu, Z., Chen, S. & Ma, X. Fundamental limitation on the detectability of entanglement. *Phys. Rev. Lett.* **129**, 230503 (2022).
44. Liu, Z. & Wei, F. Separation between entanglement criteria and entanglement detection protocols, <https://arxiv.org/abs/2403.01664> (2024).
45. Berry, D. W., Ahokas, G., Cleve, R. & Sanders, B. C. Efficient quantum algorithms for simulating sparse hamiltonians. *Commun. Math. Phys.* **270**, 359 (2007).
46. Aubrun, G. Partial transposition of random states and non-centered semicircular distributions. *Random Matrices: Theory Appl.* **1**, 1250001 (2012).
47. Calabrese, P., Cardy, J. & Tonni, E. Entanglement negativity in quantum field theory. *Phys. Rev. Lett.* **109**, 130502 (2012).
48. Lu, T.-C., Hsieh, T. H. & Grover, T. Detecting topological order at finite temperature using entanglement negativity. *Phys. Rev. Lett.* **125**, 116801 (2020).
49. Keyl, M. & Werner, R. F. Estimating the spectrum of a density operator. *Phys. Rev. A* **64**, 052311 (2001).
50. Kueng, R., Rauhut, H. & Terstiege, U. Low rank matrix recovery from rank one measurements. *Appl. Comput. Harmonic Anal.* **42**, 88 (2017).
51. Chen, S., Huang, B., Li, J., Liu, A. Sellke, M. Tight bounds for state tomography with incoherent measurements, <https://arxiv.org/abs/2206.05265> (2022).
52. Yu, X.-D., Imai, S. & Gühne, O. Optimal entanglement certification from moments of the partial transpose. *Phys. Rev. Lett.* **127**, 060504 (2021).
53. Pichler, H., Zhu, G., Seif, A., Zoller, P. & Hafezi, M. Measurement protocol for the entanglement spectrum of cold atoms. *Phys. Rev. X* **6**, 041033 (2016).
54. Wang, Y., Zhao, B. & Wang, X. Quantum algorithms for estimating quantum entropies. *Phys. Rev. Appl.* **19**, 044041 (2023).
55. Stilck França, D. & García-Patrón, R. Limitations of optimization algorithms on noisy quantum devices. *Nat. Phys.* **17**, 1221 (2021).
56. Chen, S., Cotler, J., Huang, H.-Y. & Li, J. The complexity of nisq, <https://arxiv.org/abs/2210.07234> (2022).
57. Shor, P. W. Scheme for reducing decoherence in quantum computer memory. *Phys. Rev. A* **52**, R2493 (1995).
58. Steane, A. M. Error correcting codes in quantum theory. *Phys. Rev. Lett.* **77**, 793 (1996).
59. Preskill, J. Fault-tolerant quantum computation In *Introduction to quantum computation and information* (World Scientific, 1998) pp. 213–269.
60. Terhal, B. M. Quantum error correction for quantum memories. *Rev. Mod. Phys.* **87**, 307 (2015).
61. Aharonov, D., Ben-Or, M. Fault-tolerant quantum computation with constant error. In *Proceedings of the Twenty-Ninth Annual ACM Symposium on Theory of Computing*, STOC '97 (Association for Computing Machinery, New York, NY, USA, 1997) p. 176–188.
62. Fowler, A. G., Mariantoni, M., Martinis, J. M. & Cleland, A. N. Surface codes: Towards practical large-scale quantum computation. *Phys. Rev. A* **86**, 032324 (2012).
63. Huggins, W. J. et al. Virtual distillation for quantum error mitigation. *Phys. Rev. X* **11**, 041036 (2021).
64. Koczor, B. Exponential error suppression for near-term quantum devices. *Phys. Rev. X* **11**, 031057 (2021).
65. McClean, J. R., Kimchi-Schwartz, M. E., Carter, J. & de Jong, W. A. Hybrid quantum-classical hierarchy for mitigation of decoherence and determination of excited states. *Phys. Rev. A* **95**, 042308 (2017).
66. Takagi, R. Optimal resource cost for error mitigation. *Phys. Rev. Res.* **3**, 033178 (2021).
67. Takagi, R., Endo, S., Minagawa, S. & Gu, M. Fundamental limits of quantum error mitigation. *npj Quantum Inf.* **8**, 114 (2022).
68. Chen, S., Cotler, J., Huang, H.-Y. & Li, J. Exponential separations between learning with and without quantum memory. In *IEEE 62nd Annual Symposium on Foundations of Computer Science (FOCS)* pp. 574–585 (IEEE, 2022).
69. Gilyén, A., Arunachalam, S. and Wiebe, N. Optimizing quantum optimization algorithms via faster quantum gradient computation. In *Proceedings of the 2019 Annual ACM-SIAM Symposium on Discrete Algorithms (SODA)* (Society for Industrial and Applied Mathematics, 2019) pp. 1425–1444.
70. Huggins, W. J. et al. Nearly optimal quantum algorithm for estimating multiple expectation values. *Phys. Rev. Lett.* **129**, 240501 (2022).
71. Childs, A. & Wiebe, N. Hamiltonian simulation using linear combinations of unitary operations. *Quantum Inf. Comput.* **12**, 901–924 (2012).
72. Lu, S., Ba nuls, M. C. & Cirac, J. I. Algorithms for quantum simulation at finite energies. *PRX Quantum* **2**, 020321 (2021).
73. Zhang, D.-B., Zhang, G.-Q., Xue, Z.-Y., Zhu, S.-L. & Wang, Z. D. Continuous-variable assisted thermal quantum simulation. *Phys. Rev. Lett.* **127**, 020502 (2021).
74. Motta, M. et al. Determining eigenstates and thermal states on a quantum computer using quantum imaginary time evolution. *Nat. Phys.* **16**, 205 (2020).
75. Huang, H.-Y., Kueng, R. & Preskill, J. Predicting many properties of a quantum system from very few measurements. *Nat. Phys.* **16**, 1050 (2020).
76. Elben, A. et al. The randomized measurement toolbox. *Nat. Rev. Phys.* **5**, 9 (2023).
77. Patel, D. & Wilde, M. M. Wave matrix lindbladization i: Quantum programs for simulating markovian dynamics. *Open Syst. Inf. Dyn.* **30**, 2350010 (2023).
78. Low, G. H. & Chuang, I. L. Hamiltonian Simulation by Qubitization. *Quantum* **3**, 163 (2019).
79. Martyn, J. M., Rossi, Z. M., Tan, A. K. & Chuang, I. L. Grand unification of quantum algorithms. *PRX Quantum* **2**, 040203 (2021).
80. Choi, M.-D. Completely positive linear maps on complex matrices. *Linear Algebra Appl.* **10**, 285 (1975).
81. Holevo, A. Statistical decision theory for quantum systems. *J. Multivar. Anal.* **3**, 337 (1973).
82. Helstrom, C. W. Quantum detection and estimation theory. *J. Stat. Phys.* **1**, 231 (1969).

Acknowledgements

We appreciate insightful discussions with Xiongfeng Ma, Zhenyu Cai, Jinzhao Sun, Zhaohui Wei, Jens Eisert, Otfried Gühne, and Huixuan He. Fuchuan Wei and Zhengwei Liu are supported by BMSTC and ACZSP (Grant No. Z221100002722017). Zhengwei Liu is supported by NKPs (Grant No. 2020YFA0713000), Beijing Natural Science Foundation Key Program (Grant

No. Z220002). Zhenhuan Liu and Guoding Liu are supported by the National Natural Science Foundation of China (Grant No. 12174216) and the Innovation Program for Quantum Science and Technology (Grant No. 2021ZD0300804). Zizhao Han and Dong-Ling Deng are supported by the National Natural Science Foundation of China (Grants No. 12075128 and T2225008), Tsinghua University Dushi Program, and Shanghai Qi Zhi Institute.

Author contributions

Dong-Ling Deng and Zhengwei Liu supervised the research. Fuchuan Wei and Zhenhuan Liu provided the theory. Fuchuan Wei, Zhenhuan Liu, and Dong-Ling Deng wrote the manuscript. All authors reviewed the manuscript.

Competing interests

The authors declare no competing interests.

Additional information

Supplementary information The online version contains supplementary material available at

<https://doi.org/10.1038/s41534-024-00949-z>.

Correspondence and requests for materials should be addressed to Dong-Ling Deng or Zhengwei Liu.

Reprints and permissions information is available at <http://www.nature.com/reprints>

Publisher's note Springer Nature remains neutral with regard to jurisdictional claims in published maps and institutional affiliations.

Open Access This article is licensed under a Creative Commons Attribution-NonCommercial-NoDerivatives 4.0 International License, which permits any non-commercial use, sharing, distribution and reproduction in any medium or format, as long as you give appropriate credit to the original author(s) and the source, provide a link to the Creative Commons licence, and indicate if you modified the licensed material. You do not have permission under this licence to share adapted material derived from this article or parts of it. The images or other third party material in this article are included in the article's Creative Commons licence, unless indicated otherwise in a credit line to the material. If material is not included in the article's Creative Commons licence and your intended use is not permitted by statutory regulation or exceeds the permitted use, you will need to obtain permission directly from the copyright holder. To view a copy of this licence, visit <http://creativecommons.org/licenses/by-nc-nd/4.0/>.

© The Author(s) 2024